



# Accurate modelling and analysis of battery–supercapacitor hybrid energy storage system in DC microgrid systems

C. R. Arunkumar<sup>1</sup> · Udaya Bhasker Manthati<sup>1</sup> · Punna Srinivas<sup>1</sup>

Received: 14 May 2020 / Accepted: 7 June 2021 / Published online: 26 July 2021

© The Author(s), under exclusive licence to Springer-Verlag GmbH Germany, part of Springer Nature 2021

## Abstract

Battery is considered as the most viable energy storage device for renewable power generation although it possesses slow response and low cycle life. Supercapacitor (SC) is added to improve the battery performance by reducing the stress during the transient period and the combined system is called hybrid energy storage system (HESS). The HESS operation purely depends on the control strategy and the power sharing between energy storage systems. The low pass filter based frequency sharing method is the common strategy used to share the power between the battery and SC. The HESS controller consists of two current controllers for controlling battery current and SC current and a voltage controller for regulating DC bus voltage. The quick regulation of DC bus voltage and current depends on the rapidity of operation of each control loop and the delay imposed by LPF. However, the conventional method considers only the SC characteristics for designing the outer voltage controller which leads to error in the calculated parameters. This work investigates controller design based on accurate modelling of HESS by factoring in battery converter and SC converter characteristics and the low pass filter effect. Further, the system is analyzed and compared in conditions with and without battery current loop. To verify the efficacy of the controller designed for the purpose, simulation studies are conducted in MATLAB/SIMULINK. A system prototype is developed in dSPACE 1104 platform.

**Keywords** Battery energy storage · Bidirectional DC–DC converter · Supercapacitor energy storage · HESS · PI controller · Low pass filter · Power splitting strategy

---

✉ C. R. Arunkumar  
acr\_research@student.nitw.ac.in

Udaya Bhasker Manthati  
ub@nitw.ac.in

Punna Srinivas  
srinu240@student.nitw.ac.in

<sup>1</sup> Electrical Engineering Department, National Institute of Technology, Warangal, Telangana 506004, India

## 1 Introduction

Battery has been the most popular energy storage device for the last 200 years and its performance has drastically improved in the last two decades. Its advantages make it an integral part of many applications, such as renewable energy-based power systems, automobiles, portable electronic devices and isolated power applications such as shipboard, military, etc. [1, 2]. The improvement in battery life cycle and energy density substantially helps in the development of better DC microgrid systems. However, the slow response of the battery affects the overall system performance as well as leads to deterioration of battery life under sudden changes [3, 4]. Therefore fast responsive storage devices (FRSD) are introduced in different areas along with the battery to meet the transient requirements [5].

FRSD is characterized by its high power density and long cycle life. However, FRSD cannot be used for long term applications due to its fast discharge characteristics. A combination of battery and FRSD can enhance the system response in addition to improving the battery life [6]. The available choices for FRSD along with battery in HESS are flywheel, superconducting magnetic energy storage (SMES) and SC [7]. The SMES is considered technology in nascent stages compared to flywheel and SC due to its size and expenses [8, 9]. The flywheel has the advantages of high power density, longer life and easy construction. However, it is very heavy and bulky to handle. Moreover the flywheel requires complex circuitry for energy conversion and utilization [10, 11]. On the other hand, SC possesses the advantage of smaller size, lower space occupancy and better adaptability compared to other FRSDs. For the above reasons, SC is selected as the complimentary ES for battery based HESS applications [12]. A comparative study of battery and FRSDs is given in Table 1 [7].

The SC easily absorbs the transient pressure from the microgrid when it operates along with battery. However, the battery and SC cannot be interconnected directly due to the difference in voltage levels and dynamic characteristics [12]. As a result, different combinations of battery and SC are introduced in the literature viz. (1) passive [13], (2) semi active [14, 15] and (3) fully active configurations [16, 17]. The fully active configuration is more commonly used due to its dominant characteristics in the control and utilization of ESs compared to other configurations [18].

The control layer aims to maintain the DC bus voltage constant. For that, the coordinate operation of HESS is required. Different control strategies for HESS

**Table 1** Comparative study of lead acid battery (LAB) and FRSD

S. no	Storage device	Energy density (Wh/L)	Power density (W/L)	Response time (ms)	Cycle efficiency (%)	Life time (years)	Self discharge (%/day)
1	LAB	50–300	10–500	3–20	70–83	5–15	0.1–0.4
2	Flywheel	20–200	5000–20,000	> 10	80–95	15	70–95
3	SMES	0.5–10	1000–5000	1–10	80–90	20	10–15
4	SC	5–50	5000–50,000	< 10	80–95	10–15	10–20

are proposed in the literature. In each case, the operation of HESS depends on the power allocation between battery and SC. A comprehensive review of power allocation strategies in the battery–SC system is presented in the literature [19]. Optimization-based power allocation strategies were investigated to improve HESS performance [20]. This method includes the formulation of optimization problem and cost function. The artificial neural network (ANN)-based power-sharing approach is discussed in the paper [21, 22]. This approach aims to obtain the best performance for HESS based on available data. However, the potency of the method depends on the quantity and quality of data used for training. In fuzzy based approach, power is shared based on load constraints and SOC constraints [23, 24].

The classical control strategy with low pass filter (LPF) for power-sharing between battery and SC has been meticulously researched in the literature. It consists of a cascaded PI controller with two control layers [25]. The inner control layer is devoted to the current regulation of battery and SC while the outer control layer is designed for DC bus voltage regulation and stability. For the HESS system, three PIs are required in a centralized control approach [26–28] and four PIs are required for decentralized control [29–31]. In the centralized control, a common LPF is used to split the total current into battery reference current and SC reference current. In decentralized control, the LPF is implemented as an impedance droop [29]. In all cases, the PI design is purely based on the bandwidth (BW) and phase margin requirement. The BW selection for each control loop decides the speed of the loop and operation of the overall system.

The major requirement of the two-loop control strategy is an accurate mathematical model for the design of controller parameters. In LPF based control strategy, previous studies follow the two-loop control structure where the outer loop is designed by considering the SC loop alone. The battery inner current loop is the slowest inner loop and the outer voltage loop settles only after the battery current loop settles. Hence the outer loop design must consider the complete system model for controller design. A complete modelling of the system by considering battery and SC system is presented in literature [32]. However the work focuses on the DC microgrid energy management strategy.

From the literature, it is important to note that the controller design is approximated by discarding the battery current loop to reduce complexity. The effect of both converters may be assumed to be same, when the converters are designed for the same power level. However, in most applications, the SC voltage selected such that it is more than battery voltage for better SC voltage utilization. Thus, it is important to analyze the performance of HESS by considering both battery and SC current loop as well as LPF effect. Therefore, this paper presents an accurate modelling of HESS by considering both battery and SC loop characteristics for two-loop control strategy design. The salient features of this work can be summarized as follows:

- 1 The paper proposes an accurate modelling strategy for HESS by considering both battery and SC characteristics as well as LPF effect to improve the regulation of DC microgrid.

- 2 The proposed system ensures high gain at low frequencies and low gain at switching frequencies to enhance stability of the system.
- 3 The proposed method is implemented in fully active converter topology and control parameters are compared.

The paper is organised as follows: in Sect. 2, the paper discuss the HESS-system configuration and modelling. Section 3 explains control strategy and design. Section 4 reports simulation study and results. Section 5 deals with hardware implementation and the results while Sect. 6 presents conclusions.

## 2 HESS-system configuration and modelling

In active configuration of HESS, the storage devices are connected to the DC bus through bidirectional DC-DC converters as shown in Fig. 1a [16]. The DC bus is represented by load. Battery and SC are connected to the DC bus through DC-DC boost converter. The diode is replaced with MOSFET switches to achieve bidirectional property for boost converters. Battery converter control is placed in such a

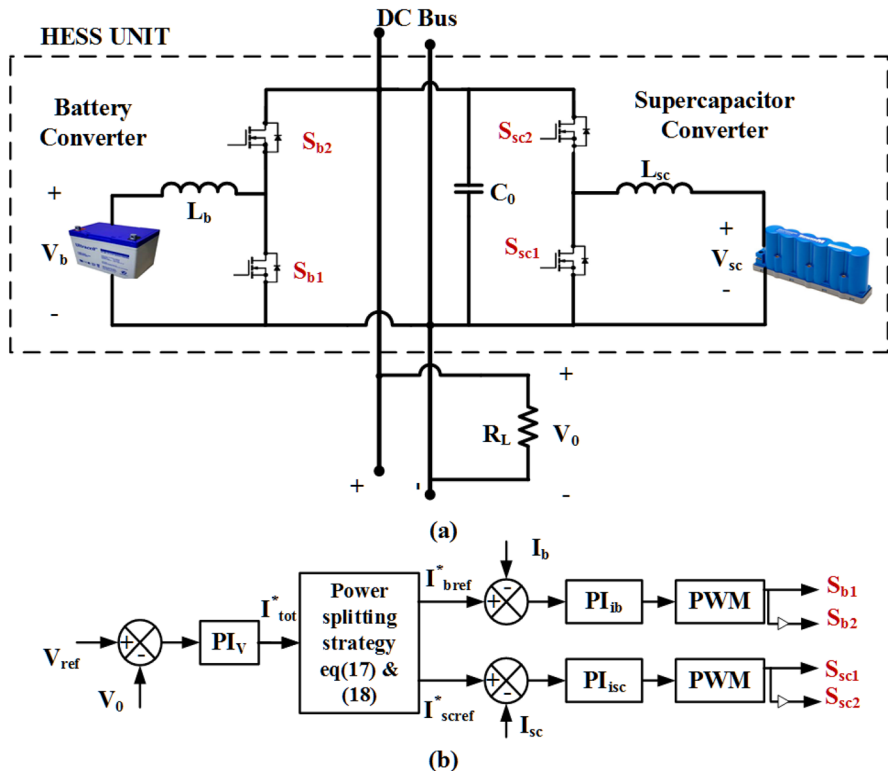


**Fig. 1** HESS: **a** active battery–SC configuration, **b** controller connection of HESS

way that it is switched on for supplying steady state power. The SC converter is switched to supply transient power. Whenever a change occurs in the DC bus, SC acts faster than the battery so that the stress on the battery is reduced. As a result, the power at DC bus is maintained constant and the disturbance is mitigated as fast as possible.

## 2.1 Battery energy storage system

The battery plays an important role in the operation of HESS as it provides continuous power to the DC bus. The mathematical model of lead acid battery is adopted from mathworks as shown in Fig. 2a [33, 34]. Battery operation depends on the SOC of the battery and the SOC variation of battery is much slower as compared to SC. For the safety of energy storage system, SOC kept in the range of  $20\% < \text{SOC} < 80\%$ . The battery model equations are given in Eqs. (1), (2) and (3) [26].

$$E_{bat} = E_0 - K \frac{Q}{i_b t - 0.1 \cdot Q} (i_b t + i_b^*) + \text{Exp}(t) \quad (1)$$

$$V_{bat} = E_{bat} - i_b R_{bat} \quad (2)$$

$$\dot{Exp}(t) = B \cdot |i(t)| \cdot (-\text{Exp}(t) + A \cdot u(t)) \quad (3)$$

where  $i_b$  = battery current (A),  $i_b^*$  = filtered battery current (A),  $\text{Exp}$  is the exponential zone voltage of battery (V), and  $Q$  = battery capacity (Ah),  $R_{bat}$  = battery internal resistance ( $\Omega$ ),  $A$  = exponential voltage (V),  $B$  = exponential capacity ( $Ah^{-1}$ ),  $i_b t$  = actual battery charge.

## 2.2 SC energy storage system

Supercapacitor is considered as the connecting bridge between the normal capacitor and batteries. The fast responding nature with a capacitance of a few hundred farads makes SC suitable for transient applications. The SC model available on mathworks [35, 36] is used for SC analysis. The SC mathematical model is a combination of

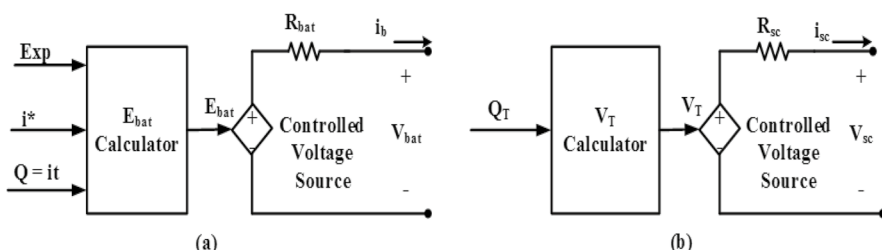


Fig. 2 Mathematical model of **a** lead acid battery [32], **b** supercapacitor [34]

Helmholtz model and Gouy–Chapman model. SC internal voltage and SOC equations are given by Eqs. (4), (5) and (6).

The maximum energy stored in SC is given by

$$E_{sc,max} = \frac{1}{2} C_{sc} V_{sc,max}^2 \quad (4)$$

The energy stored by the SC at any instant,  $E_{sc}(t)$  is given by

$$E_{sc}(t) = \frac{1}{2} C_{sc} V_{sc}^2(t) \quad (5)$$

The energy and SOC of SC are related to as follows:

$$SOC_{sc} = \frac{E_{sc}(t)}{E_{sc,max}} \quad (6)$$

Hence the SOC of SC shows the variation of energy from time to time. Hence SOC is given in terms of charge is shown in Eq. (7) [35],

$$SOC_{sc} = \frac{Q_{int} - \int_0^t i(\tau) d\tau}{Q_T} \quad (7)$$

SC mathematical model is derived from these equations and is shown in Fig. 2b. Where  $Q_T$  and  $V_T$  are the total internal charge (Coulomb) and voltage (V) of SC and is given by Eqs. (8) and (9), respectively.

$$Q_T = \int i_{sc}(t) dt \quad (8)$$

$$V_T = \frac{N_s Q_T d}{N_p N_e \epsilon \epsilon_0 A_r} + \frac{2 N_e N_s R T}{F} \sinh^{-1} \frac{Q_T}{N_p N_e^2 A_r \sqrt{8 R T \epsilon \epsilon_0 c}} \quad (9)$$

where  $\epsilon$  = permittivity of electrolyte material (Farad/m),  $\epsilon_0$  = permittivity of free space (Farad/m),  $N_s$  = number of SC connected in series,  $N_p$  = number of SC connected in parallel,  $N_e$  = number of electrode layers,  $R$  = ideal gas constant,  $T$  = operating temperature,  $c$  = molar concentration ( $\text{mol}/\text{m}^3$ ),  $Q_T$  = total charge of SC unit,  $d$  = thickness of Helmholtz layer (m),  $i_{sc}$  = SC current.

## 2.3 Energy storage converter system

The HESS system consist of two boost converter as mentioned earlier. Both converters possess bi-directional properties. Though the design focusses on the boost capability because of the presence of right hand zero in boost converter, it operates in continuous conduction mode (CCM). For the design of converters, inductor ripple current is taken as 5% and capacitor voltage ripple is considered as 2%. The system is designed for 72 W. Also the design equations are developed from conventional boost converter analysis

[37]. The equations for voltage across inductor and current through capacitor are given by Eqs. (10) and (11).

$$L \frac{di_L(t)}{dt} = V_s \quad (10)$$

$$C \frac{dv_0(t)}{dt} = \frac{-V_0}{R_L} \quad (11)$$

### 2.3.1 Battery converter design

The aim of the battery boost converter is to supply steady state power to the DC bus. Hence the converter is designed to deliver maximum load power. A 12 V, 7 ampere-hour lead-acid battery is considered for this application. The advantage of lead-acid battery is that the voltage drop during discharging is very low. Therefor the converter is designed for rated 12 V of battery. The converter design equations shown in Eqs. (12) and (13) and are derived from Eqs. (10) and (11).

$$L_b = \frac{V_0 D_b}{\Delta i_{Lb} f_{sw}} \quad (12)$$

where  $f_{sw}$  is the switching frequency and  $D_b$  represents the battery converter duty ratio. Similarly the output capacitor filter can be obtained by the equation below:

$$C_{0b} = \frac{V_0 D_b}{\Delta v_0 R_L f_{sw}} \quad (13)$$

$V_0$  and  $\Delta v_0$  are the output voltage and allowable output voltage ripple.

### 2.3.2 SC converter design

The design of SC bidirectional dc–dc converter is similar to the design of battery converter. However the design specifications are different. Considering the previous literature, the converter is designed for maximum SC voltage. This method gives good response at high SC voltage since 75% of energy stored in a capacitor is available above 50% of SC voltage. The converter design equations are given by:

$$L_{sc} = \frac{V_0 D_{sc}}{\Delta i_{Lsc} f_{sw}} \quad (14)$$

and

$$C_{0sc} = \frac{V_0 D_{sc}}{\Delta v_0 R_L f_{sw}} \quad (15)$$

The design values are given in Table 2. The  $C_0$  combines the total effect of both battery output capacitor  $C_{0b}$  and SC output capacitor  $C_{0sc}$ .

**Table 2** System parameters for simulation and hardware implementation

S. no	Parameters	Values
1	Battery input voltage, $V_b$	12 V
2	SC input voltage, $V_{sc}$	16 V
3	Load resistance, $R_L$	8 $\Omega$
4	Battery boost converter inductance, $L_b$	2 mH
5	SC boost converter inductance, $L_{sc}$	1.80 mH
6	Total output capacitance, $C_0 = C_{0sc} + C_{0b}$	250 $\mu\text{F}$
7	Output power, $P_{out}$	72 W
8	Switching frequency, $f_{sw}$	20 kHz
9	Output voltage, $V_0$	24 V
10	Nominal power for Hardware	30 W

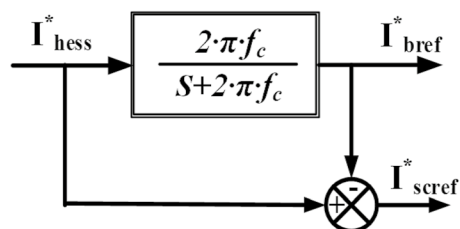
### 3 Control strategy and controller design

The control strategy for HESS focuses mainly on power sharing between the battery and the SC. The accurate tuning of control parameters decides the operation ranges on the system. In this section, control strategy, modelling and design of accurate HESS system and controller tuning are presented. The first step towards the controller design is the small signal modelling (SSM) of the converter system. Based on SSM, the controller is designed by combining the action of both battery and SC converter.

#### 3.1 Control strategy

The LPF plays an important role in power sharing in HESS. The reference current generation with respect to LPF is shown in Fig. 3. In LPF control strategy, the LPF splits the total current reference into high frequency component and average component. The cutoff frequency of LPF is selected as 31 rad/s so as to reduce system delay [25]. Here ' $f_c$ ' represents the LPF cutoff frequency and relevant equations are given in Eqs. (16), (17) and (18).

**Fig. 3** LPF based power splitting strategy for HESS



$$LPF = \frac{2 \cdot \pi \cdot f_c}{s + 2 \cdot \pi \cdot f_c} \quad (16)$$

If the total current in the system is  $I_{tot}$ , then reference current for battery and SC is given by

$$I_{Lb,ref} = I_{tot} \cdot \frac{2 \cdot \pi \cdot f_c}{s + 2 \cdot \pi \cdot f_c} \quad (17)$$

and

$$I_{sc,ref} = I_{tot} \cdot \left(1 - \frac{2 \cdot \pi \cdot f_c}{s + 2 \cdot \pi \cdot f_c}\right) \quad (18)$$

### 3.2 Small signal modeling of boost converters

The first step towards the controller design is small signal analysis of the converters. The controller parameters are designed using MATLAB/SISO tool with the help of transfer functions derived from small signal analysis. The equations averaged for inductor voltage and current through capacitor in the boost converter over one switching period are given by Eqs. (19) and (20).

$$L_x \frac{di_{Lx}(t)}{dt} = v_x - (1 - d_x)v_{cx} \quad (19)$$

$$C_{0x} \frac{dv_{cx}(t)}{dt} = (1 - d_x)i_{Lx} - \frac{v_{cx}}{R_L} \quad (20)$$

Based on the inductor and capacitor equations, different transfer functions for the converter are derived using state space averaging technique [36]. The voltage control transfer functions is derived as

$$G_{vdx} = \frac{\hat{v}_{0x}(s)}{\hat{d}_x(s)} = \frac{(1 - D_x)V_0 - L_x I_{Lx}s}{L_x C_{0x}s^2 + \frac{L_x}{R_L}s + (1 - D_x)^2} \quad (21)$$

Also the current control transfer function is calculated as

$$G_{idx} = \frac{\hat{i}_{Lx}(s)}{\hat{d}_x(s)} = \frac{C_{0x}V_0s + 2(1 - D_x)I_{Lx}}{L_x C_{0x}s^2 + \frac{L_x}{R_L}s + (1 - D_x)^2} \quad (22)$$

Output transfer impedance for the converter can be derived from (21) and (22) as

$$G_{vix} = \frac{\hat{v}_0(s)}{\hat{i}_{Lx}(s)} = \frac{(1 - D_x)V_0 - L_x I_{Lx}s}{C_{0x}V_0s + 2(1 - D_x)I_{Lx}} \quad (23)$$

### 3.3 Analysis of accurate design of control system

Based on the SSM, the controller block diagram designed for the purpose is shown in Fig. 4. As mentioned earlier, the system performance depends on both converter parameters. Hence the controller design requires an accurate model of HESS system. First we design the inner current control loop by considering the slow dynamics of the battery and fast dynamics of SC. Then the voltage control loop is designed to maintain the DC bus voltage constant. All PI values are assigned with the help of MATLAB/SISO tool box.

#### 3.3.1 Battery inner current control loop design

The control diagram of the battery inner current loop,  $G_{ib,cl}$  is shown in Fig. 4b.  $G_{ib}$  represents the duty to current transfer function and  $G_{ib,cl}$  is the overall closed current loop transfer function of battery.  $H_1 = 1$  since the system is designed for unity feedback control. As said earlier, the bandwidth of inner current loop is always made higher than outer voltage control loop to eliminate switching ripple. Battery current control loop is designed for a lower bandwidth of  $\frac{2\pi f_{sw}}{12}$  to prevent the battery from responding to transient currents.

The loop gain of battery current control loop is given by

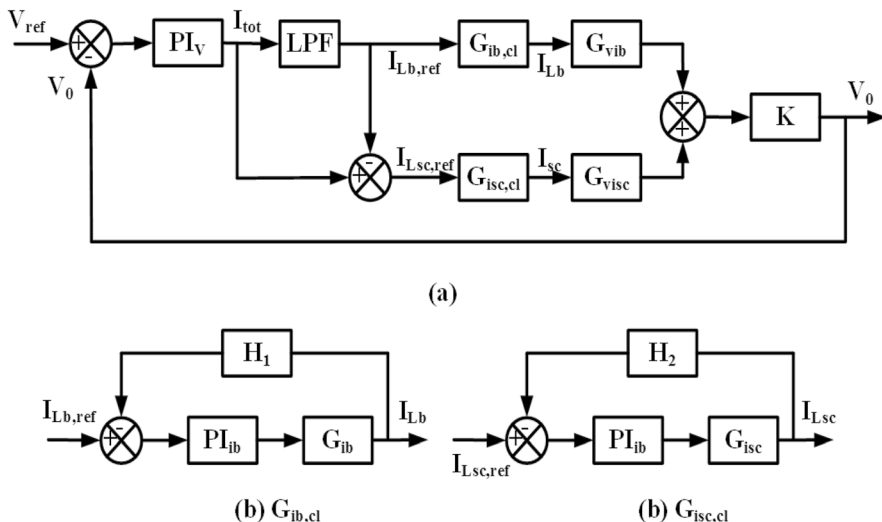


**Fig. 4** Accurate SSM of **a** overall system, **b** inner battery current loop, **c** inner SC current loop

$$G_{idbl} = PI_{ib} \cdot G_{idb} \cdot H_1 \quad (24)$$

and the closed loop current control loop transfer function is

$$G_{idb,cl} = \frac{PI_{ib} \cdot G_{idb}}{1 + (PI_{ib} \cdot G_{idb} \cdot H_1)} \quad (25)$$

The PI compensator that regulates the battery current is given by

$$PI_{ib} = K_{pib} + \frac{K_{iib}}{s} \quad (26)$$

$K_{pib}$  and  $K_{iib}$  are the proportional and integral gains to regulate battery current. The PI values are tuned for a gain margin of 10 db and PM of  $60^\circ$  [25]. The bode diagram of corresponding compensated system is shown in Fig. 5a.

### 3.3.2 SC inner current control loop design

The aim of the SC current control loop is to control the charging and discharging SC current.  $H_2 = 1$  since the system is unity feedback system. It is very pertinent to conclude that the selection of BW decides the operation of SC. The BW is selected higher than the battery current control loop and is less than  $f_{sw}$ . The selected BW is  $\frac{2\pi f_{sw}}{8}$  with PM of  $60^\circ$ . The loop gain of SC current control loop is given by

$$G_{idscl} = PI_{isc} \cdot G_{idsc} \cdot H_2 \quad (27)$$

and the closed loop current control loop transfer function is

$$G_{idsc,cl} = \frac{PI_{isc} \cdot G_{idsc}}{1 + (PI_{isc} \cdot G_{idsc} \cdot H_2)} \quad (28)$$

The controller for SC current loop is given by

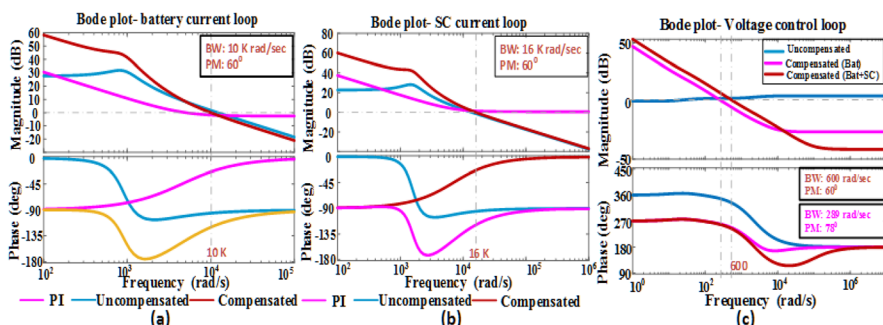


**Fig. 5** Bode plot for different control loops **a** SC current loop, **b** battery current loop, **c** outer voltage loop

$$PI_{isc} = K_{pisc} + \frac{K_{iisc}}{s} \quad (29)$$

The  $K_{pisc}$  and  $K_{iisc}$  are the proportional and integral gains respectively to regulate SC current. The calculated  $PI_{isc}$  gains are given in Table 3. It is clearly seen that the fast nature of SC current loop is reflected in the PI values of SC current loop, since  $K_{iisc}$  is much higher than that of battery current loop  $K_{iib}$ . Bode diagram of the corresponding compensated system is shown in Fig. 5b.

### 3.3.3 Outer voltage control loop design

Outer voltage control loop needs more precautions in the analysis of HESS. This is because the right hand zero (RHZ) effect of boost converter can add initial boost to the system and may lead to instability at starting. Hence, unlike the previous works, the performance of both converters is considered for the design of the outer voltage control loop. Firstly, the PM and BW for the outer loop cannot be increased simultaneously. Hence the BW is limited to obtaining adequate stability. For the design of outer voltage controller, the inner current loop gain is considered as unity [28]. The overall loop transfer function for the combined system obtained from accurate modelling is given by  $G_{all}$ ,

$$G_{all} = PI_v \cdot (LPF \cdot G_{vib} + (1 - LPF) \cdot G_{visc}) \cdot K \quad (30)$$

where K represents the voltage gain of combined system, and  $K = 1/2$ . The total transfer function  $G_{all}$  is equal to  $PI_v \cdot G_{visc}$  when  $G_{vib} = G_{visc}$ . This condition is satisfied only when the voltage rating of SC and battery are equal. However in most applications, the battery and SC are rated with different voltage range. This affects the overall transfer function obtained and affects the controller parameters. The outer voltage controller is given by:

$$PI_v = K_{pv} + \frac{K_{iv}}{s} \quad (31)$$

In Fig. 5c, the blue line shows the uncompensated system, red line shows the proposed model based design with PM of  $60^\circ$  and BW of 600 rad/s. The

**Table 3** PI Controller parameters and comparison with approximate and accurate model

S. no	Control loop	PI values	PM and BW
1	Inner battery current loop	$K_{pib} = 0.744$ $K_{iib} = 2673$	BW = 10 krad/s PM = $60^\circ$
2	Inner SC control loop	$K_{pisc} = 1.069$ $K_{iisc} = 7464$	BW = 16 krad/s PM = $60^\circ$
3	<b>Outer voltage loop</b> (Approximate model)	$K_{pv} = 0.028$ $K_{iv} = 220$	BW = 289 rad/s PM = $78^\circ$
4	<b>Outer voltage loop</b> (Accurate model)	$K_{pv} = 0.005$ $K_{iv} = 449.6$	BW = 600 rad/s PM = $60^\circ$

pink line represents the bode plot for PI values with conventional method acting on combined system. It is clear that for the combined system the speed of the loop is reduced considerably when applying the PI values obtained from SC-loop alone. The PI values and comparison are shown in Table 3. The voltage control loop values shows the variation in parameters due to modelling. It is clear from the PI values that the accurate model is faster than approximate model. Further from the bode diagram, the accurate model ensures high gain at low frequencies and low gain at switching frequencies, which is important in stability considerations.

## 4 Simulation results

To verify the control and operation of battery–SC HESS, simulations were conducted in Matlab/Simulink. The simulation parameters are shown in Table 2. During simulation, SOC limits of the battery and SC were calculated and found to be under the limits. The main aim of HESS is to reduce the stress on battery and improve system performance. Hence the simulation mainly focusses on the operation of SC to support battery as well as load performance. To verify the operation, source and load disturbances were applied.

### 4.1 Performance of system under source disturbances

To test the system under source variation, the battery is replaced with a controlled DC source. At  $t = 0.3$  s, the source voltage is increased from 12 to 16 V and at 0.8 s, the source is reduced to 11 V. Again the disturbance is created at  $t = 1.2$  s and  $t = 1.6$  s as shown in Fig. 6a. The DC bus voltage shows little ripples and settles down quickly as shown in Fig. 6b. At  $t = 1.2$  s, 6 V disturbance is applied at the source voltage and removed at  $t = 1.5$  s. The test DC source power, SC power and corresponding load power are shown in Fig. 6c. To analyze the performance of HESS, it is important to check the current drawn from source and SC. Figure 6d shows the input current of DC source, SC current and load current. Compared to battery, DC source is fast varying and it introduced a little transient in the source current. From Fig. 6d, it is clear that SC is taking the transient current and supporting the battery to supply less ripple current. When the input voltage increases, the boost converter draws only limited quantity of current from the source. Further, the SC absorbs the change in power such that the sudden change in DC source power is lowered. Similarly when input current reduces, SC supplies the initial current so that battery can take enough time to discharge.

### 4.2 Performance of system under load change

The HESS is characterized by fast response towards any change in the system. Hence the best way to test HESS is through the load disturbances. To test the system, load changes are introduced by adding additional loads to the system. The load current is increased in steps of 1 A up to 3 A and then reduced in steps of 1 A. The

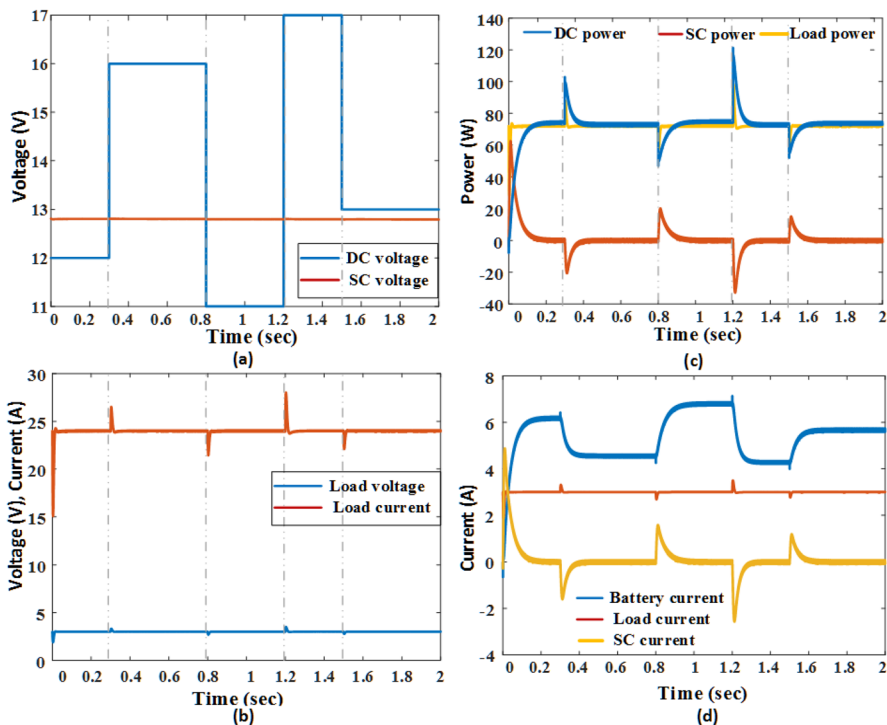


**Fig. 6** Dynamic performance of system during sudden change in source; **a** source disturbance, **b** DC power, load power and SC power, **c** Load voltage and load current, **d** battery current, SC current and load current

system maintained the DC bus voltage at 24 V and the load current varies accordingly as shown in Fig. 7a. At the time of load increment, battery current increases slowly and SC discharges to meet the initial transient current. Further it is relevant to note that the load current settle fast as compared to battery current. When the load decreases at  $t = 1.2$  s and  $t = 1.5$  s, the SC charges and makes the battery change the states slowly. The total load current supplied by battery and SC is shown in Fig. 7b. The SC supplies current at the transient period and the average current is zero for steady state operation. The load power and power delivered by HESS are shown in Fig. 7c. The variation of SC voltage is also very less which shows that it can supply transient power for longer periods. The corresponding voltage waveforms of ESS are shown in Fig. 7d.

## 5 Hardware implementation and discussion

The hardware is designed and implemented with the help of dSPACE 1104 platform and is shown in Fig. 8. The PI values obtained from accurate modelling are used for the closed loop implementation of the system. The nominal power is selected as 30

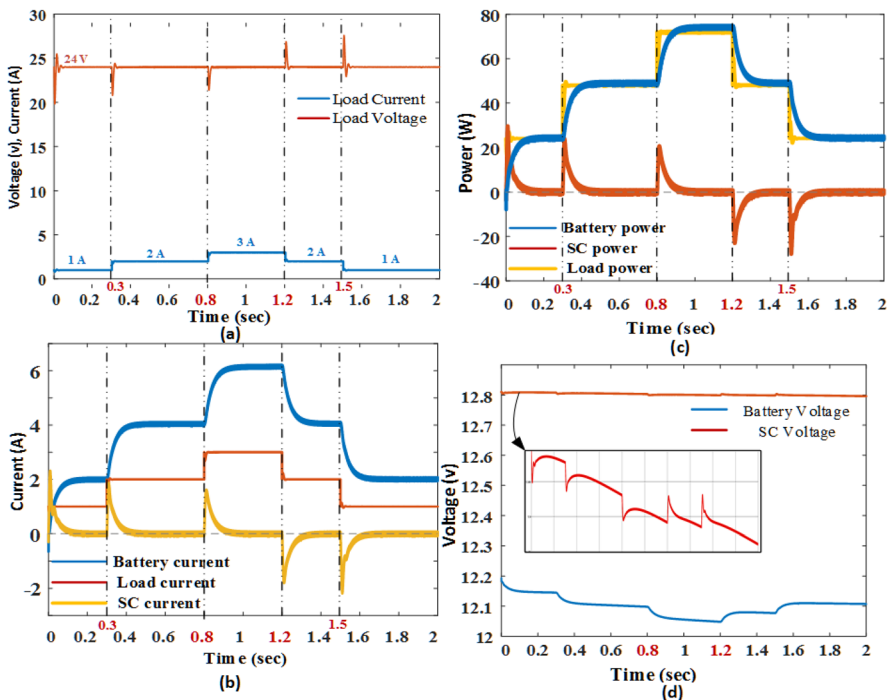


**Fig. 7** Dynamic performance of system during sudden change in load; **a** load voltage and load current, **b** battery current, SC current and load current, **c** DC power, load power and SC power, **d** battery voltage and SC voltage

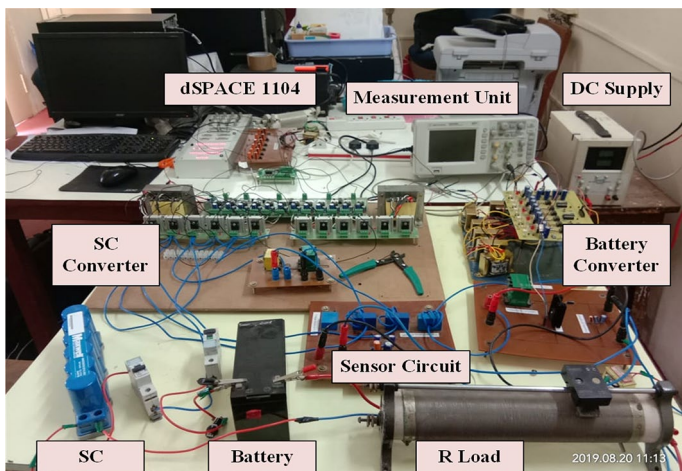


**Fig. 8** Experimental setup for HESS

W to verify the controller action. The SC operation is verified by introducing source and load disturbance in the DC bus. The load disturbance is created by adding a resistor in parallel to the main load through controlled switch. The turn on and turn off of the manual switch created disturbance as shown in Fig. 9a. In hardware development, the SC current direction is taken as negative for discharging. As a result, SC current waveform shows negative at the time of load increment and shows positive at the time of load decrement. The wave form clearly shows that load voltage is maintained at 20 V irrespective of the changes in load. During load disturbance, load current is varied from 0.6 to 1 A and SC discharges accordingly. The battery current, load current and SC current are compared in Fig. 9c, d. The magnified portion of current shows that battery current is responding slow as compared to SC current and load current. Here, load current changes from 0.6 to 1 A and the battery current changes from 1.2 to 2 A.

To verify the controller, the system is analysed with source variation by replacing the battery with regulated power supply. The corresponding load voltage, source voltage, source current, and SC current are shown in Fig. 9b. Initially, the source is increased from 10 to 16 V and reduced back to 10 V after some time. It can be seen that the source current is reduced to make the load power constant. Further, SC

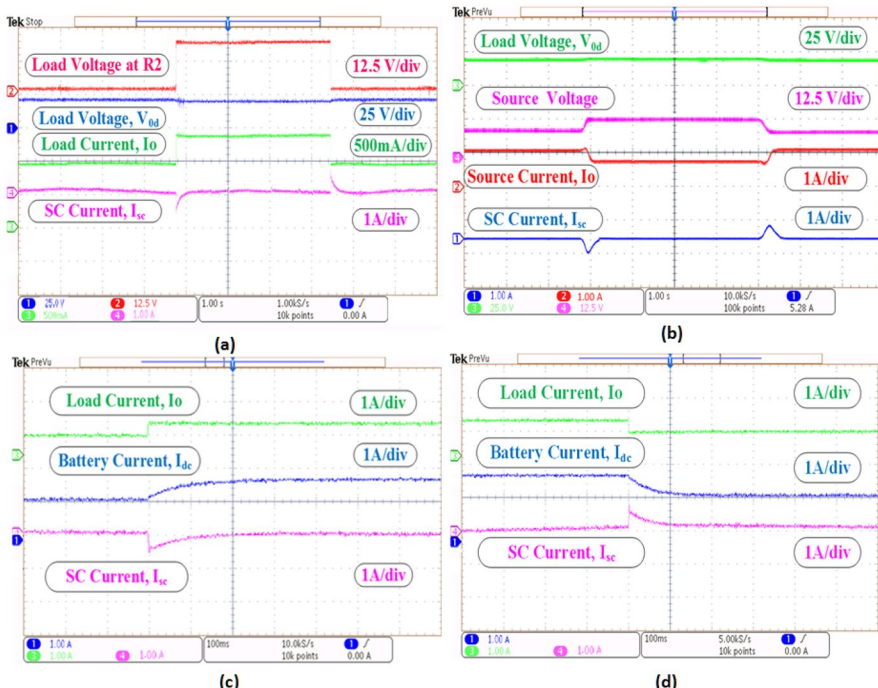


**Fig. 9** Different wave forms during load disturbance **a** Load voltage, voltage across load disturbance, load current and SC current under load disturbance, **b** Load voltage, source voltage, source current, SC current under source disturbance, **c**, **d** comparison of battery current, SC current and load current under load disturbance

discharged/charged depends on the transient nature. However, the variation is slower compared to load variation due to the manual change in source voltage. The experimental study shows that the transient occur due to source and load variations in the system is absorbed by the SC and DC bus voltage is maintained within the limits.

## 6 Conclusion

This paper presented a complete modelling of battery–SC hybrid energy storage system for DC microgrid applications. The combination of SC with battery is used to improve the system response and to enhance battery life. The efficient operation of HESS depends on the control strategy and the power sharing between ESS. In the classic control theory, PI-LPF control strategy is used to regulate the DC bus voltage along with HESS current regulation. The selection of PI gains decides the rapidity and accuracy of the system and is calculated based on the system model. In this paper, a combined modelling of HESS is designed by considering low pass filter effect as well as the effect of inner current loops. The advantage of the proposed method is that it provides enough bandwidth for the outer loop so that faster settling of DC bus voltage is ensured. For tuning the controller parameters, PM and BW are considered the main constraints. The inner current loop BW is made higher to achieve a fast response in the system. The outer control loop design involves a trade-off between BW and PM due to the presence of RHZ. The PI values obtained based on accurate model show fast response and better stability from frequency domain analysis. The PI values designed are tested under different disturbances in the system. The simulation and experimental results shows that the DC bus voltage is constant under all disturbances. The SC voltage waveform shows that it is capable of taking sudden disturbances in the system. The PI values selected on the basis of an accurate model show better band width and high gain at low frequency in bode plot compared to approximate model, which is important for stability and rapid response.

### Declarations

**Conflict of interest** The authors declare that they have no conflict of interest

## References

1. Yang, Y., Qin, Y., Tan, S.C., Hui, S.Y.R.: Efficient improvement of photovoltaic-battery systems in standalone DC microgrids using a local hierarchical control for the battery system. *IEEE Trans. Power Electron.* **34**(11), 10796–10807 (2019)
2. Belabbas, B., Allaoui, T., Tadjine, M., et al.: Power management and control strategies for off-grid hybrid power systems with renewable energies and storage. *Energy Syst.* **10**, 355–384 (2019)
3. Ibanez, F.M., et al.: Extending the autonomy of a battery for electric motorcycles. *IEEE Trans. Veh. Technol.* **68**, 4 (2019)
4. Choudhury, T.R., Nayak, B., De, A., et al.: A comprehensive review and feasibility study of DC-DC converters for different PV applications: ESS, future residential purpose, EV charging. *Energy Syst.* **11**, 641–671 (2020)

5. Akram, U., Nadarajah, M., Shah, R., Milano, F.: A review on rapid responsive energy storage technologies for frequency regulation in modern power systems. *Renew. Sustain. Energy Rev.* **120**, 109626 (2020)
6. Hajighasri, S., Salemnia, A., Hamzeh, M.: Hybrid energy storage system for microgrids applications: a review. *J. Energy Stor.* **21**, 543–570 (2019)
7. Bocklisch, T.: Hybrid energy storage approach for renewable energy applications. *J. Energy Stor.* **8**, 311–319 (2016)
8. Sun, Q., Xing, D., Alafnan, H., Pei, X., Zhang, M., Yuan, W.: Design and test of a new two-stage control scheme for SMES-battery hybrid energy storage systems for microgrid applications. *Appl. Energy* **253**, 113529 (2019)
9. Naderi, P., Fallahi, F.: A novel structure proposal for distributed generation using SMES and PV system with relative controllers design. *Energy Syst.* **6**, 153–172 (2015)
10. Azizi, I., Radjeai, H.: A new strategy for battery and supercapacitor energy management for an urban electric vehicle. *Electr. Eng.* **100**, 667–676 (2018)
11. Arani, A.A.K., Gharehpetian, G.B., Abedi, M.: A novel control method based on droop for cooperation of flywheel and battery energy storage systems in islanded microgrids. *IEEE Syst. J.* **14**(1), 1080–1087 (2019)
12. Joshi, M.C., Susovon, S.: Improved energy management algorithm with time-share-based ultracapacitor charging/discharging for hybrid energy storage system. *IEEE Trans. Ind. Electron.* **66**(8), 6032–6043 (2018)
13. Xiong, R., Chen, H., Wang, C., Sun, F.: Towards a smarter hybrid energy storage system based on battery and ultracapacitor—a critical review on topology and energy management. *J. Clean. Prod.* **202**, 1228–1240 (2018)
14. Asensio, M., et al.: Efficiency and performance analysis of battery-ultracapacitor based semi-active hybrid energy systems for electric vehicles. *IEEE Latin Am. Trans.* **16**, 10 (2018)
15. Zhang, Q., Li, G.: Experimental study on a semi-active battery-supercapacitor hybrid energy storage system for electric vehicle application. *IEEE Trans. Power Electron.* **35**(1), 1014–1021 (2019)
16. Arunkumar, C. R., Udaya B.M.: Design and small signal modelling of battery-supercapacitor HESS for DC microgrid. *TENCON 2019-2019 IEEE Region 10 Conference (TENCON)*. IEEE (2019)
17. Punna, S., Manthati, U.B., Chirayarkil Raveendran, A.: Modeling, analysis, and design of novel control scheme for two-input bidirectional DC–DC converter for HESS in DC microgrid applications. *Int. Trans. Electr. Energy Syst.* **20**, e12774 (2021)
18. Oriti, G., Norma, A., Alexander, L.J.: Hybrid energy storage control in a remote military microgrid with improved supercapacitor utilization and sensitivity analysis. *IEEE Trans. Ind. Appl.* **55**, 5 (2019)
19. Sun, L., Feng, K., Chapman, C., Zhang, N.: An adaptive power-split strategy for battery-supercapacitor powertrain-design, simulation, and experiment. *IEEE Trans. Power Electron.* **32**(12), 9364–9375 (2017)
20. Zhang, L., et al.: Multiobjective optimal sizing of hybrid energy storage system for electric vehicles. *IEEE Trans. Veh. Technol.* **67**(2), 1027–1035 (2017)
21. Varghese, N., Reji, P.: Energy storage management of hybrid solar/wind standalone system using adaptive neuro-fuzzy inference system. *Int. Trans. Electr. Energy Syst.* **29**(7), e12124 (2019)
22. Faria, J., Pombo, J., Calado, M.D.R., Mariano, S.: Power management control strategy based on artificial neural networks for standalone PV applications with a hybrid energy storage system. *Energies* **12**(5), 902 (2019)
23. Khan, M.M.S., Faruque, M.O., Newaz, A.: Fuzzy logic based energy storage management system for MVDC power system of all electric ship. *IEEE Trans. Energy Convers.* **32**(2), 798–809 (2017)
24. Bhosale, R., Vivek, A.: Fuzzy logic control of the ultracapacitor interface for enhanced transient response and voltage stability of a dc microgrid. *IEEE Trans. Ind. Appl.* **55**(1), 712–720 (2018)
25. Tummuru, N.R., Mishra, M.K., Srinivas, S.: Dynamic energy management of renewable grid integrated hybrid energy storage system. *IEEE Trans. Ind. Electron.* **62**(12), 7728–7737 (2015)
26. Manandhar, U., Ukil, A., Gooi, H.B., Tummuru, N.R., Kollimalla, S.K., Wang, B., Chaudhari, K.: Energy management and control for grid connected hybrid energy storage system under different operating modes. *IEEE Trans. Smart Grid* **10**(2), 1626–1636 (2017)
27. Krishan, O., Suhag, S.: A novel control strategy for a hybrid energy storage system in a grid-independent hybrid renewable energy system. *Int. Trans. Electr. Energy Syst.* **30**(4), e12262 (2020)
28. Kollimalla, S.K., Mishra, M.K., Narasamma, N.L.: Design and analysis of novel control strategy for battery and supercapacitor storage system. *IEEE Trans. Sustain. Energy* **5**(4), 1137–1144 (2014)

29. Xu, Q., Hu, X., Wang, P., Xiao, J., Tu, P., Wen, C., Lee, M.Y.: A decentralized dynamic power sharing strategy for hybrid energy storage system in autonomous DC microgrid. *IEEE Trans. Ind. Electron.* **64**(7), 5930–5941 (2016)
30. Chen, X., Zhou, J., Shi, M., Yan, L., Zuo, W., Wen, J.: A novel virtual resistor and capacitor droop control for HESS in medium-voltage DC system. *IEEE Trans. Power Syst.* **34**(4), 2518–2527 (2019)
31. Lin, P., Wang, P., Xiao, J., Wang, J., Jin, C., Tang, Y.: An integral droop for transient power allocation and output impedance shaping of hybrid energy storage system in DC microgrid. *IEEE Trans. Power Electron.* **33**(7), 6262–6277 (2017)
32. Kotra, S., Mishra, M.K.: Design and stability analysis of DC microgrid with hybrid energy storage system. *IEEE Trans. Sustain. Energy* **10**(3), 1603–1612 (2019)
33. Mathworks. Implement generic battery model-Simulink-MathWorks United Kingdom. <http://www.mathworks.co.uk/help/physmod/powersys/ref/battery.html>. Accessed 09 Feb 2020
34. Tremblay, O., Dessaint, L.A.: Experimental validation of a battery dynamic model for EV applications. *World Electr. Veh. J.* **3**(2), 289–298 (2009)
35. Mathworks. Implement generic supercapacitor model-Simulink-MathWorks India. <https://in.mathworks.com/help/physmod/sps/powersys/ref/supercapacitor.html>. Accessed 09 Feb 2020
36. Oldham, K.B.: A Gouy–Chapman–Stern model of the double layer at a (metal)/(ionic liquid) interface. *J. Electroanal. Chem.* **613**(2), 131–138 (2008)
37. Erickson, R.W., Maksimovic, D.: *Fundamentals of Power Electronics*. Springer, Berlin (2017)

**Publisher's Note** Springer Nature remains neutral with regard to jurisdictional claims in published maps and institutional affiliations.